Cancer Research

Targeted Methylation of Two Tumor Suppressor Genes Is Sufficient to Transform Mesenchymal Stem Cells into Cancer Stem/Initiating Cells

I-Wen Teng, Pei-Chi Hou, Kuan-Der Lee, et al.

Cancer Res 2011;71:4653-4663. Published OnlineFirst April 25, 2011.

Published OnlineFirst April 25, 2011; DOI:10.1158/0008-5472.CAN-10-3418

Targeted Methylation of Two Tumor Suppressor Genes Is Sufficient to Transform Mesenchymal Stem Cells into Cancer Stem/Initiating Cells

I-Wen Teng[1], Pei-Chi Hou[1], Kuan-Der Lee[2], Pei-Yi Chu[3], Kun-Tu Yeh[3], Victor X. Jin[4], Min-Jen Tseng[1], Shaw-Jenq Tsai[5], Yu-Sun Chang[6], Chi-Sheng Wu[6], H. Sunny Sun[7], Kuen-daw Tsai[1,8], Long-Bin Jeng[8], Kenneth P. Nephew[9], Tim H.-M. Huang[10], Shu-Huei Hsiao[1], and Yu-Wei Leu[1]

Abstract

Although DNA hypermethylation within promoter CpG islands is highly correlated with tumorigenesis, it has not been established whether DNA hypermethylation within a specific tumor suppressor gene (TSG) is sufficient to fully transform a somatic stem cell. In this study, we addressed this question using a novel targeted DNA methylation technique to methylate the promoters of *HIC1* and *RassF1A*, two well-established TSGs, along with a two-component reporter system to visualize successful targeting of human bone marrow–derived mesenchymal stem cells (MSC) as a model cell system. MSCs harboring targeted promoter methylations of *HIC1*/*RassF1A* displayed several features of cancer stem/initiating cells including loss of anchorage dependence, increased colony formation capability, drug resistance, and pluripotency. Notably, inoculation of immunodeficient mice with low numbers of targeted MSC resulted in tumor formation, and subsequent serial xenotransplantation and immunohistochemistry confirmed the presence of stem cell markers and MSC lineage in tumor xenografts. Consistent with the expected mechanism of TSG hypermethylation, treatment of the targeted MSC with a DNA methyltransferase inhibitor reversed their tumorigenic phenotype. To our knowledge, this is the first direct demonstration that aberrant TSG hypermethylation is sufficient to transform a somatic stem cell into a fully malignant cell with cancer stem/initiating properties. *Cancer Res; 71(13); 4653–63. ©2011 AACR.*

Introduction

DNA methylation, a tightly regulated process during normal development, frequently becomes dysregulated during disease development including cancer (1–3). Although methylation-induced tumorigenesis has yet to be recapitulated experimentally, during somatic cell proliferation, environmental and extracellular signals can initiate changes in DNA methylation that contribute to clonal selection, altered cellular behavior, and ultimately tumorigenesis (4–6). Hypomethylation and/or hypermethylation of specific loci, including tumor suppressor loci, were strongly associated with transformation and carcinogenesis (7, 8), and genetic knockout of the DNA methyltransferases (DNMT), resulted in global hypomethylation and tumorigenesis (9, 10). Although a causative role for altered methylation at specific loci, particularly as an initiating neoplastic event, remains poorly understood, dormant stem cells, either pre-existing in tissues or arising from somatic cells, may play a role in cancer origin and prognosis (4). Furthermore, because DNA hypermethylation of tumor suppressor gene (TSG) has been documented in many cancers, and its spreading correlates with cancer progression (4), we hypothesized that abnormal DNA hypermethylation can disrupt somatic stem cell proliferation and differentiation, resulting in the development of neoplasia.

To directly examine the effect of aberrant DNA methylation on cellular physiology, we established a Targeted DNA Methylation method called "TDM" (11, 12), in which transfection established an *in vitro* methylated DNA complementary to the target gene promoter region initiated recruitment of DNMT to the endogenous target loci. Consequently, DNMT-mediated methylation spreads within the promoter region of the target loci, ultimately silencing the target gene after cellular passages.

Authors' Affiliations: [1]Human Epigenomics Center, Department of Life Science, Institute of Molecular Biology and Institute of Biomedical Science, National Chung Cheng University; [2]Chang Gung Memorial Hospital, Chia-Yi; [3]Department of Pathology, Changhua Christian Hospital, Changhua, Taiwan; [4]Department of Biomedical Informatics, The Ohio State University Columbus, Ohio; [5]Department of Physiology, [6]Institute of Molecular Medicine, College of Medicine, National Cheng Kung University, Tainan; [7]Basic Medical Sciences, Chang Gung University, Tao-Yuan; [8]Department of Internal Medicine, China Medical University Beigang Hospital, Yunlin, Taiwan; [9]Medical Sciences and Department of Cellular and Integrative Physiology, Indiana University Simon Cancer Center, School of Medicine, Bloomington, Indiana; and [10]Division of Human Cancer Genetics, Department of Molecular Virology, Immunology, and Medical Genetics, and the Comprehensive Cancer Center, The Ohio State University, Columbus, Ohio

Note: Supplementary data for this article are available at Cancer Research Online (http://cancerres.aacrjournals.org/).

I-W. Teng and P.-C. Hou contributed equally to this work.

Corresponding Author: Shu-Huei Hsiao, National Chung Cheng University, 168 University Road, Min Hsiung, Chia-Yi, 621 Taiwan. Phone: 886-5-2720411 ext 53202; Fax: 886-5-2722871; E-mail: bioshh@ccu.edu.tw or Yu-Wei Leu, ext 66507; E-mail: bioywl@ccu.edu.tw

doi: 10.1158/0008-5472.CAN-10-3418

Published OnlineFirst April 25, 2011; DOI:10.1158/0008-5472.CAN-10-3418

To monitor progression of TDM and cellular transformation, we also developed a 2-component system (11, 12). The first component consisted of regulation of tetracycline repressor (*Tet*) expression by the cloned target promoter sequence. A *CMV* promoter driving expression of a reporter (enhanced green fluorescence protein or EGFP) comprised the second component. A *Tet* repressor binding site, *Tet operator*, placed between the *CMV* and the *EGFP*, regulated EGFP expression. In the absence of DNA methylation, *Tet* expression was observed, and the expression of EGFP was silenced. Induction of DNA methylation silenced the Tet repressor and activated EGFP expression, allowing us to observe progression of DNA methylation in a living cell. Furthermore, if target loci DNA methylation was sufficient to induce cellular transformation, an EGFP-expressing cell behaved like a tumor (11, 12). It was of interest to use this system to initiate TDM in a somatic stem cell and monitor the subsequent effects on cellular transformation. Although spontaneous transformation of human mesenchymal stem cells (MSC) *in vitro* was recently described (13, 14), genetic disruptions of the p53 pathway, but not retinoblastoma (Rb), was sufficient to transform a fat-derived MSC (15), supporting the possibility that sarcoma could be initiated from MSC.

In the current study (work flow is illustrated in Supplementary Fig. S1A), we aimed to test the hypothesis that targeted DNA methylation is sufficient for cellular transformation, thus the promoter regions of *HIC1* (hypermethylated in cancer 1) and *RassF1A* (ras-associated family protein isoforms 1A), 2 TSGs reported to be frequently silenced by DNA methylation in cancer (16–18), were cloned, methylated *in vitro,* and then transfected into the MSCs, individually or concurrently. *HIC1* and *RassF1A* are involved in highly diverse, interacting cellular networks (16, 19, 20), and their loss of function could result in the recently described phenomenon of oncogenic addiction through p53 pathway (5). We thus hypothesized that hypermethylation of *HIC1* and *RassF1A* would not only to directly suppress their tumor suppressor function but also disrupt multiple cellular networks resulting in tumorigenesis and cancer progression.

Materials and Methods

MSC isolation and characterization

Human MSC isolation and culture were carried out as described by Lee and colleagues (21). MSC expansion medium, passages, and culture condition were as described by Hsiao and colleagues (11).

In vitro DNA methylation

Four micrograms of PCR-amplified *HIC1* and *RassF1A* promoters were incubated with 20 units of CpG methyltransferase (New England BioLabs) at 37°C for 4 hours in the presence of 160 μmol/L *S*-adenosylmethionine to induce methylation.

Validation of *in vitro* DNA methylation

Methylated DNA showing resistance to methylation-sensitive restriction enzymes (*Bst*UI) indicated completed conversion (Supplementary Fig. S2).

Cy5 labelling of the *HIC1* promoter fragment

HIC1 DNA was labeled with *Label*IT tracker Reagents (Mirus) according to the manufacturer's instruction.

Transfection

The methylated PCR products (0.4 μg) were denatured at 95°C and then transfected into 5×10^5 cells using DMRIE-C (Invitrogen), according to the manufacturer's instructions. Unmethylated PCR products were transfected as control. Cells were transfected three times at days 1, 3, and 5.

Semiquantitative real-time methylation-specific PCR

The semiquantitative methylation-specific PCR (qMSP) experiment was conducted and products were quantified according to the protocol described in Yan and colleagues (22). Briefly, bisulfite-converted genomic DNAs (0.5 μg) were subject to real-time PCR (RT-PCR) with methylation-specific primers (Supplementary Table S2). The qMSP reactions were carried out using the SYBR Green I PCR Kit (Toyobo) in an iQ5 Real-Time PCR instrument (Bio-Rad). Melting analysis was conducted followed by all of the PCR reactions to ensure a specific amplicon was generated. *Col2A1* was used for standard curve construction and as loading control. Serial dilution of *Col2A1* amplified bisulfite-converted DNA was used to generate standard curve. Methylation percentage was calculated as follows: (means of target gene)/(means of *Col2A1*); fold change was calculated as follows: (TDM methylation percentage)/(mock methylation percentage). Endogenous and exogenous *HIC1* promoters were discerned by the reverse primers indicated in Supplementary Figures S1B and S3A.

Differential methylation hybridization

All procedures for the differential methylation hybridization (DMH) microarray were conducted as described in Leu and colleagues (18) using a human CpG island microarray (Agilent). Briefly, *me_H&R*-treated and control MSC genomic DNAs were digested into small fragments and then ligated with designed adaptors. Methylation-sensitive restriction enzymes (*Bst*UI and *Hpa*II) were used to discriminate the methylated and the unmethylated DNA fragments. Differences in methylation status were then amplified by PCR using the adaptor as primer. The amplicons from control and *me_H&R*-transfected cells were labeled with Cy3 and Cy5, respectively and then cohybridized onto the CpG microarray. After measuring the Cy3 and Cy5 intensity, the *M* value [$M = \log_2$ (Cy5 intensity/Cy3 intensity)] was used to indicate the difference in DNA methylation between 2 sources, and the *L* value [$L = 0.5 \times \log_2$ (Cy5 $\times$ Cy3)] was used to indicate the intensity of individual loci. Both values were adjusted and normalized by LOWESS. A cutoff value of 4 based on the *M* value was used to identify the target loci.

Immunostaining

Cells were fixed in 2% formaldehyde/PBS, then permeabilized with 0.5% NP40/PBS. After blocked with horse serum/PBS (1:100), the slides were incubated with primary antibody in 3% bovine serum albumin (BSA)/PBS followed by 3 times of PBS washes. The cells were incubated with secondary

Published OnlineFirst April 25, 2011; DOI:10.1158/0008-5472.CAN-10-3418

antibodies conjugated with Fluorescein or Texas Red (Vector Lab) in 3% BSA/PBS. After several PBS washes, the slides were mounted in mounting medium with 4′,6-diamidino-2-phenylindole (DAPI; Vector Lab). The primary antibodies used were as follows: anti-HIC1 (Millipore), anti-RassF1A (Bioscience), anti-CD133 (Abcam), anti-Oct4 (Cell Signaling), and anti-Neuronal nuclei (NeuN; Chemicon).

5-Aza-dc-2′-deoxycytidine treatment

Control and *me_H&R* transfected MSCs were treated with 20 μmol/L (Fig. 1) or 5 μmol/L (Supplementary Fig. S6D) of 5-aza-dc-2′-deoxycytidine (5-aza-dc) or an equal final volume of dimethyl sulfoxide (DMSO) for 5 consecutive days.

Cloning of the human *HIC1* and *RassF1A* promoters

Primer sequences for human *HIC1* and *RassF1A* promoters are listed in Supplementary Table S1. Genomic DNA purified from human MSCs served as a template for PCR. Purified PCR products were ligated into the *pyT&A* cloning vector (Yeastern Biotech) according to the manufacturer's protocol. Inserts were confirmed by restriction digests and sequencing. Cloning and TDM for the Salvador–Warts–Hippo (SWH) signaling pathway components were conducted using the same protocols and the primers were listed in Supplementary Table S1.

Semiquantitative RT-PCR

Total RNA isolation, first-strand cDNA synthesis, and detection of the transcripts were carried out as described (18). Briefly, total RNA (2 μg) was reverse transcribed using the SuperScript III reverse transcriptase (Invitrogen). The semiquantitative RT-PCR (qRT-PCR) was then carried out by SYBR Green I PCR Kit (Toyobo) in an iQ5 Real-Time PCR instrument (Bio-Rad). A serial dilution of glyceraldehyde-3-phosphate dehydrogenase (*GAPDH*)-amplified cDNA was used as control to generate standard curve and *GAPDH* from each samples was used as loading control. The primers are listed in Supplementary Table S2.

Cell survival assay

In 96-well plates, 20 μL of MTT solution (Sigma-Aldrich; 5 mg/mL) was added to each well containing different number of cells and incubated at 37°C for 5 hours. The reaction was

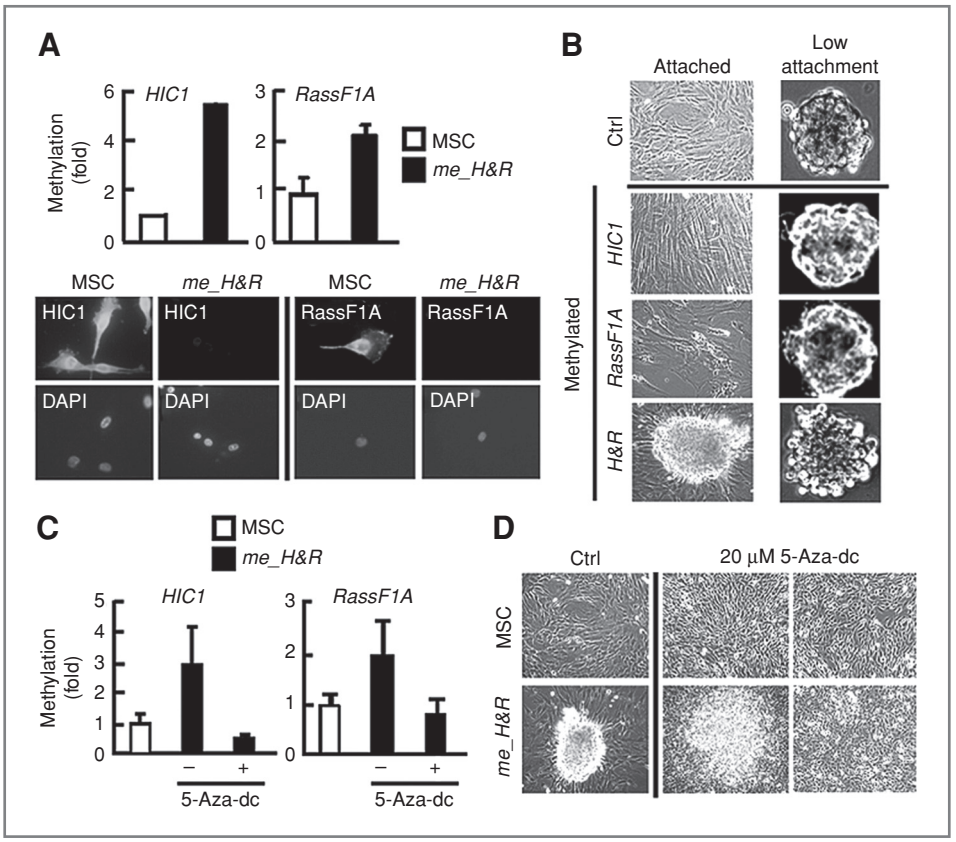

Figure 1. Concurrent *HIC1* and *RassF1A* methylation in transformed MSCs. A, *HIC1* and *RassF1A* TDM. Denatured methylated or unmethylated (mock control) *HIC1* and/or *RassF1A* promoter DNAs were transfected individually or together into human MSCs. The promoter methylation of endogenous *HIC1* (top left) and endogenous *RassF1A* (top right) were detected by qMSP and protein expression was detected by immunostaining (bottom). B, transformation of MSCs by concurrent *HIC1* and *RassF1A* methylation. MSCs transfected with unmethylated DNA only (control), *me_HIC1*, *me_RassF1A*, or *me_H&R* were cultured in attachment (left) or low attachment dishes (right). Spheroid formation was observed for all 4 treatments on low attachment dishes; however, only the *me_H&R* MSCs showed loss of contact inhibition. C, 5-aza-dc treatment reverses *me_H&R*-induced endogenous *HIC1* and *RassF1A* hypermethylation as measured by qMSP. D, 5-aza-dc treatment represses *me_H&R*-induced MSC aggregates. Loss of DNA methylation after 5-aza-dc treatment was correlated with reversion of the loss of contact inhibition phenotype in *me_H&R* treated MSCs (right bottom).

Published OnlineFirst April 25, 2011; DOI:10.1158/0008-5472.CAN-10-3418

terminated by adding 200 μL of DMSO, and absorbance was measured at 595 nm.

Soft agar assay

Cells were plated at a density of 5×10^4 per well in soft agar. After 2 weeks of culture, cells were stained with 0.01% crystal violet, and the number of spheres (>50 cells) from each dish was counted.

Transwell study

Cells were plated at a density of 5×10^4 per well into the hanging cell culture insert (Millipore), and the redistribution of the cells on the other side of the insert was observed, stained, and quantified.

In vivo tumorigenesis and serial transplantation of xenografts

Six-week-old nude mice (Narl: ICR-*Foxn1*^{nu}) were inoculated subcutaneously with 1×10^4*me_H&R*-transfected or control MSCs. Growth of tumours was monitored until they reached 0.8 cm in diameter. Then, tumors were surgically removed and subcultured in MSC medium on low attachment plates until spheres were observed again. The same number of subcultured cells was inoculated into a new nude mouse, and the entire procedure ($n = 9$) was repeated 4 more times ($n = 36$ in total).

Immunohistochemistry

Tumor masses surgically removed from nude mice inoculated with *me_H&R*-transfected MSCs were paraffin embedded and sectioned at 4 μm or embedded in optimum cutting temperature (OCT) and sectioned on a cryostat (Leica) at 12 μm. Sections were stained with the indicated antibodies, and detection was carried out with Vectastain (Vector Lab) for the paraffin sections and Fluorescein- or Texas red–conjugated anti-mouse or rabbit IgG (Vector Lab) for the cryosections, followed by DAPI staining. Sections were also stained with hematoxylin and eosin (H&E; Vector Lab) for pathologic exams.

Lineage-specific induction of MSCs

Transfected MSCs (mock or *me_H&R*) were plated onto 6-well plates at 5×10^4 cells per well. After attachment, the medium was replaced with neuronal preinduction medium [Dulbecco's modified Eagle's media (DMEM) with 20% FBS, 10 ng/mL basic fibroblast growth factor (bFGF), and 1 mmol/L β-mercaptoethanol] for 24 hours, followed by neuronal induction medium [DMEM with 100 μmol/L butylated hydroxyanisole (BHA), 10 μmol/L forskolin, 2% DMSO, 25 mmol/L KCl, 2 mmol/L valproic acid, 1 × B27 supplement, 10 ng/mL bFGF, 10 ng/mL platelet-derived growth factor (PDGF)]. Morphologic changes and NeuN expression were used to validate neuronal induction. Osteocyte induction medium consisted of DMEM, 10% FBS, 10 mg/mL penicillin/streptomycin, 100 nmol/L dexamethasone, 10 mmol/L β-glycerophosphate, and 50 μmol/L L-ascorbic acid-2-phosphate. Cells were treated with the osteocyte induction medium for 10 days and then subject to alkaline phosphatase (Sigma-Aldrich) staining.

Construction of two-component reporter system

The construction of *HIC1* 2-component reporter system is described and illustrated in Supplementary Figure S4. Both constructs were sequence validated and used to transfect the MSCs and transfected cells were selected with hygromycin and G418 resistance. PCR were carried out to validate the integrations of both constructs (*HIC1-TR* and *EG1*; Supplementary Fig. S4B). MSC clones carrying both reporter constructs were treated with doxycycline (Supplementary Fig. S4B). Doxycycline-induced EGFP expression indicates the reporter system is functional.

Human subjects

Isolation and characterization of human MSCs were conducted under Institutional Review Board (IRB) regulations of the Chang Gung Memorial Hospital.

Animals

The use of mice followed the regulations and protocols reviewed and approved by the Institutional Animal Care and Use Committee at the National Chung Cheng University.

Results

Targeted *HIC1* and *RassF1A* methylation transforms MSCs

In vitro methylated (validation of *in vitro* methylation is shown in Supplementary Fig. S2) or unmethylated (control) *HIC1* and *RassF1A* promoter DNA fragments were transfected into human bone marrow–derived MSCs mixed population (MSC_MP) alone or in combination. Transfection of methylated *HIC1* (*me_HIC1*) or methylated *RassF1A* (*me_RassF1A*) increased endogenous *HIC1* or *RassF1A* promoter methylation, as detected by qMSP (Fig. 1A, top). MSP amplification was confirmed by sequencing in Supplementary Fig. S3A and B) and the expression of endogenous *HIC1* or *RassF1A* decreased accordingly, as detected by immunostaining (Fig. 1A, bottom). TDM was confirmed by bisulfite sequencing (Supplementary Fig. S3C and D).

Loss of contact inhibition was used as a screening criterion for MSC transformation (Fig. 1B, left). Transfection and selection of transformed MSCs are illustrated in Supplementary Figure S6A. Cotransfection of methylated *HIC1* and *RassF1A* (*me_H&R*) caused formation of anchorage-independent aggregates, similar to the transformed phenotype in attached cultures, whereas the controls and cells transfected with either *me_HIC1* or *me_RassF1A* alone remained contact inhibited (Fig. 1B, left middle two). When cultured in low attachment dishes, both methylated- and mock-transfected MSCs formed spherical aggregates (Fig. 1B, right), suggesting that these *me_H&R* transfected MSCs retained their self-renewal property.

To confirm that loss of anchorage dependence was due to DNA hypermethylation, cells were treated with the DNMT inhibitor 5-aza-dc. 5-Aza-dc treatment decreased the hypermethylation level of endogenous *HIC1* and *RassF1A* in the *me_H&R*-transfected MSCs (Fig. 1C and Supplementary Fig. S6D) and abrogated the formation of *me_H&R*-induced

Published OnlineFirst April 25, 2011; DOI:10.1158/0008-5472.CAN-10-3418

aggregates (Fig. 1D, right and Supplementary Fig. S6D, top). These data indicate that DNA hypermethylation of both *HIC1* and *RassF1A* potentially transformed somatic MSCs and rendered them anchorage independent. Moreover, the requirement for methylation of both *HIC1* and *RassF1A* for MSC transformation supports the notion that cancer initiation and development is a multistep process.

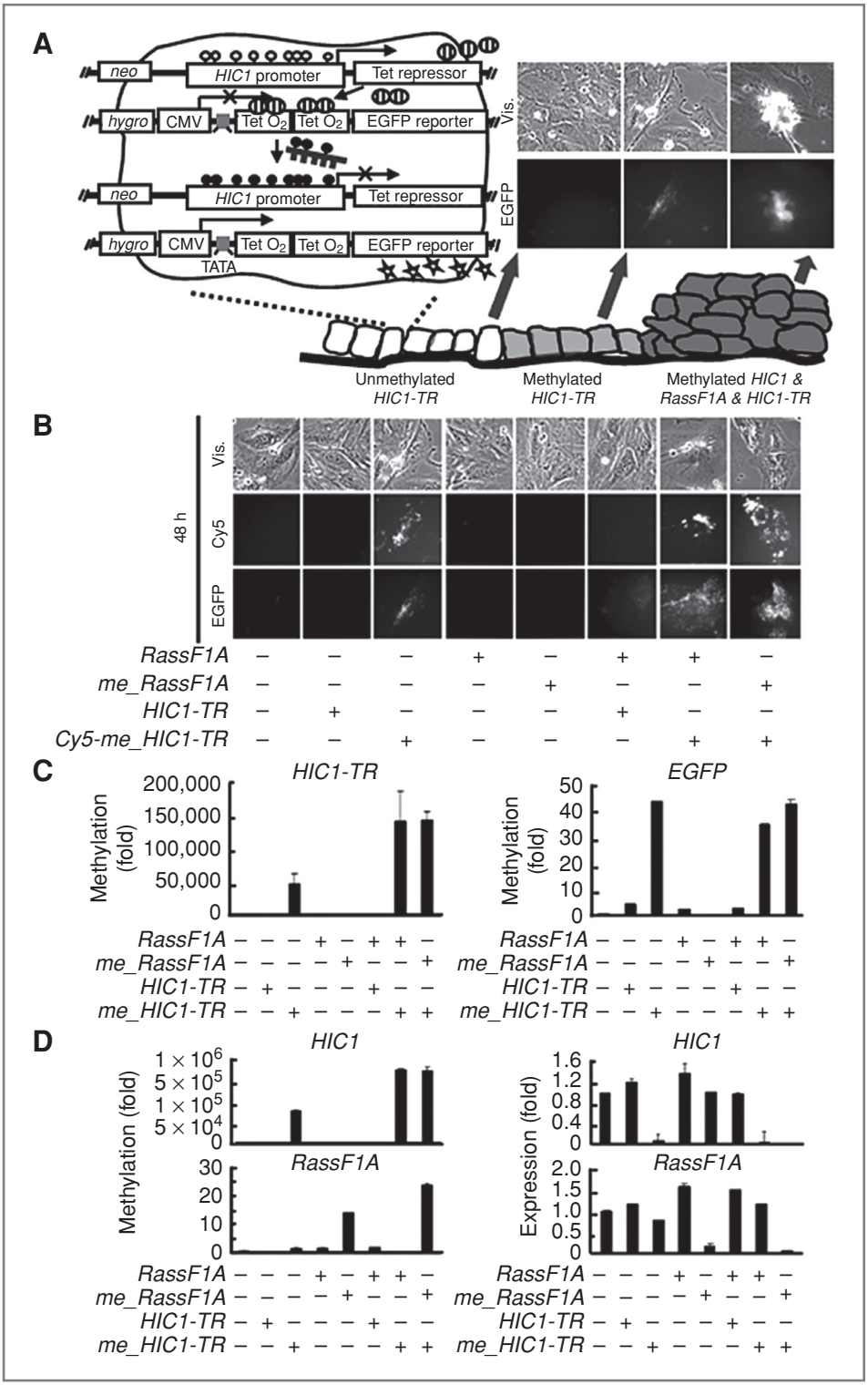

Figure 2. Visualization of targeted DNA methylation and MSC transformation. A, schematic diagram of the reporter system (left; construction and validation of the obtained clones in Supplementary Fig. S4). Targeted *HIC1* methylation was visualized by EGFP fluorescence (right middle) including *RassF1A* TDM led to EGFP-expressing cell aggregation (right). B, tracking TDM. Unmethylated (control) and/or methylated *HIC1* and *RassF1A* DNA fragments were transfected into the MSCs harboring both constructs shown in A. *me_HIC1* was labeled with Cy5 to track the distribution of transfected DNA in the MSCs, after induction of EGFP expression. Only the Cy5-containing cells expressed EGFP, confirming the specificity of the targeted methylation. C, detecting the methylation state of the exogenous *HIC1* promoter (*HIC1-TR*) and the expression of *EGFP*. qMSP was carried out to quantify exogenous *HIC1* promoter region methylation using *HIC1*-specific and vector-specific primers (left). Increased *HIC1-TR* methylation was observed only in the *me_HIC1*-targeted MSCs. *EGFP* expression increased accordingly, as detected by qRT-PCR (right). D, validation of *HIC1* and/or *RassF1A* TDM. MSCs were treated with methylated *HIC1* and/or *RassF1A* as C. qMSP was used to detect methylation changes at endogenous *HIC1* or *RassF1A* promoter (left). qRT-PCR was used to determine changes in expression of endogenous *HIC1* or *RassF1A* (right).

Published OnlineFirst April 25, 2011; DOI:10.1158/0008-5472.CAN-10-3418

Validation of TDM by two-component reporter system

To confirm that the TDM caused silencing at the transcriptional level and induced aggregates within the targeted cells, we used a 2-component reporter system (11, 12) to mark and track methylation-mediated silencing of the *HIC1* promoter in live cells (single colonies, SC). In this system, the *HIC1* promoter regulates expression of the *EGFP* reporter construct (Fig. 2A flow diagram on left; reporter system construction is illustrated in Supplementary Fig. S4). Methylation of the *HIC1* promoter alone did not result in phenotypic changes but caused *HIC1* promoter silencing, as indicated by increased *EGFP* expression (Fig. 2A, right middle). However, concomitant methylation of *RassF1A* and *HIC1* led to cell aggregates containing EGFP-expressing (i.e., *HIC1* silenced) cells (Fig. 2A, right and Supplementary Fig. S6B and C).

To track the distribution of transfected DNAs, *me_HIC1* construct was labeled with Cy5 prior to transfection. Cy5 signals localized mainly in the nuclear region (Fig. 2B and Supplementary Fig. S5), indicating that the *me_HIC1* entered the MSC nuclei. EGFP was detected in these Cy5-containing/transfected MSC (Fig. 2B, columns 3, 7, 8). When *me_HIC1* was used to transfect the cells, qMSP analysis further showed increased methylation of exogenous *HIC1* promoter (*HIC1-TR*; Fig. 2C, left), and EGFP expression increased accordingly (Fig. 2C, right). The *me_RassF1A, RassF1A*, or control (unmethylated) *HIC1* DNAs failed to induce the EGFP expression, further indicating that we successfully and specifically methylated the *HIC1* promoter. Targeted *HIC1* methylation had no effect on the methylation state of the endogenous *RassF1A* promoter and vice versa (Fig. 2D), consistent with our previous report that the TDM is locus-specific (11, 12). Combined transfection of *me_HIC1* and *me_RassF1A* resulted in methylation of both endogenous loci, as determined by qMSP (Fig. 2D, left), as well as concomitant silencing of both genes (qRT-PCR; Fig. 2D, right). Data from the 2-component reporter system further confirmed that our targeting method caused gene silencing at the transcriptional level and that aberrant DNA methylation of both *HIC1* and *RassF1A* might transform

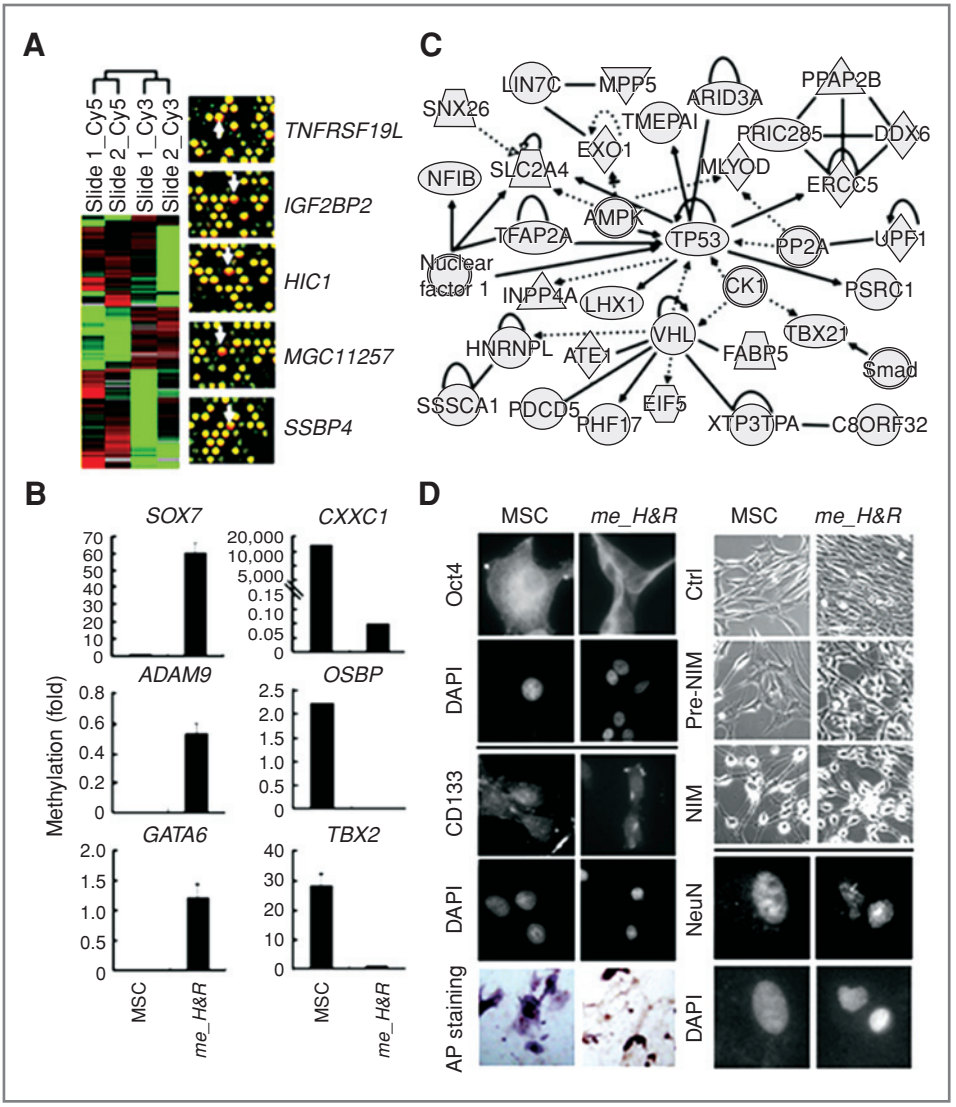

Figure 3. Methylation changes and stemness of *me_H&R*-transfected MSCs. A, left, altered methylation levels of the MSC methylome depicted by the heatmap of the DMH data. Mock-transfected cells were labeled with Cy3, *me_H&R*-transfected cells were labeled with Cy5. Red and green lines correspond to hyper- and hypomethylation, respectively. Right, arrows highlight hypermethylated genes in selected array blocks. B, validation of altered methylation by qMSP. C, visualization of affected loci by unsupervised pathway finding (PathVisio; ref. 44). D, stemness of *me_H&R*-transfected MSCs. Immunostaining for Oct4 and CD133 stem cell markers (top left). Phase contrast and immunostaining of MSCs during neuronal induction (right) and osteocyte induction (bottom left). pre-NIM, neuronal preinduction medium; NIM, neuronal induction medium. The neuronal differentiation was indicated by NeuN immunostaining. AP, alkaline phosphatase.

Published OnlineFirst April 25, 2011; DOI:10.1158/0008-5472.CAN-10-3418

normal somatic stem cells. Furthermore, our data indicated that methylation of *HIC1* initiated the accumulation of epigenetic changes in MSCs and increased the potential for transformation. In normal cells, the transformation process can be prohibited by gatekeepers or roadblocks, such as *RassF1A*; thus, gatekeeper silencing can allow for excess cell proliferation and/or genome corruption, increasing the probability of neoplastic transformation.

Transfection of *me_H&R* induces genome-wide DNA methylation changes in MSC

To further investigate changes in DNA methylation following *me_H&R* targeting, genome-wide methylation profiling of *me_H&R*-transfected and control MSCs was carried out using DMH microarrays (23). As shown in the methylation heatmap, transfection of *me_H&R* induced extensive disruption in the MSC epigenome (Fig. 3A, left). Individual loci (Fig. 3A, right) displaying hypermethylation (*SOX7*, *ADAM9*, and *GATA6*) or hypomethylation (*CXXC1*, *OSBP*, and *TBX2*) were validated by qMSP (Fig. 3B). On the basis of the wide range of cellular functions associated with HIC1 and RassF1A (16, 19, 24), it was not surprising to observe global changes in the MSC methylome. Furthermore, as both *HIC1* and *RassF1A* were reported to function as TSGs that act via p53, we conducted unsupervised ontological analysis of the array target loci and found that p53 and its associated signaling components were significantly altered by *me_H&R* transfection (Fig. 3C and Supplementary Fig. S7, target loci with the p53 binding domain are listed in Supplementary Table S3). Our finding that MSC transformation is strongly associated with altered p53 function is consistent with a previous report using genetic approaches (15).

Characteristics of *me_H&R*-transformed MSCs

To determine whether the *me_H&R*-transformed MSCs retained stemness, *me_H&R* transfected MSCs were labeled with antibodies against stem cell surface markers CD133 and Oct4 and induced to differentiate. Expression levels of CD133 and Oct4 were unaffected by *me_H&R* transfection (Fig. 3D, top left). Multipotency was assayed by neuronal induction and

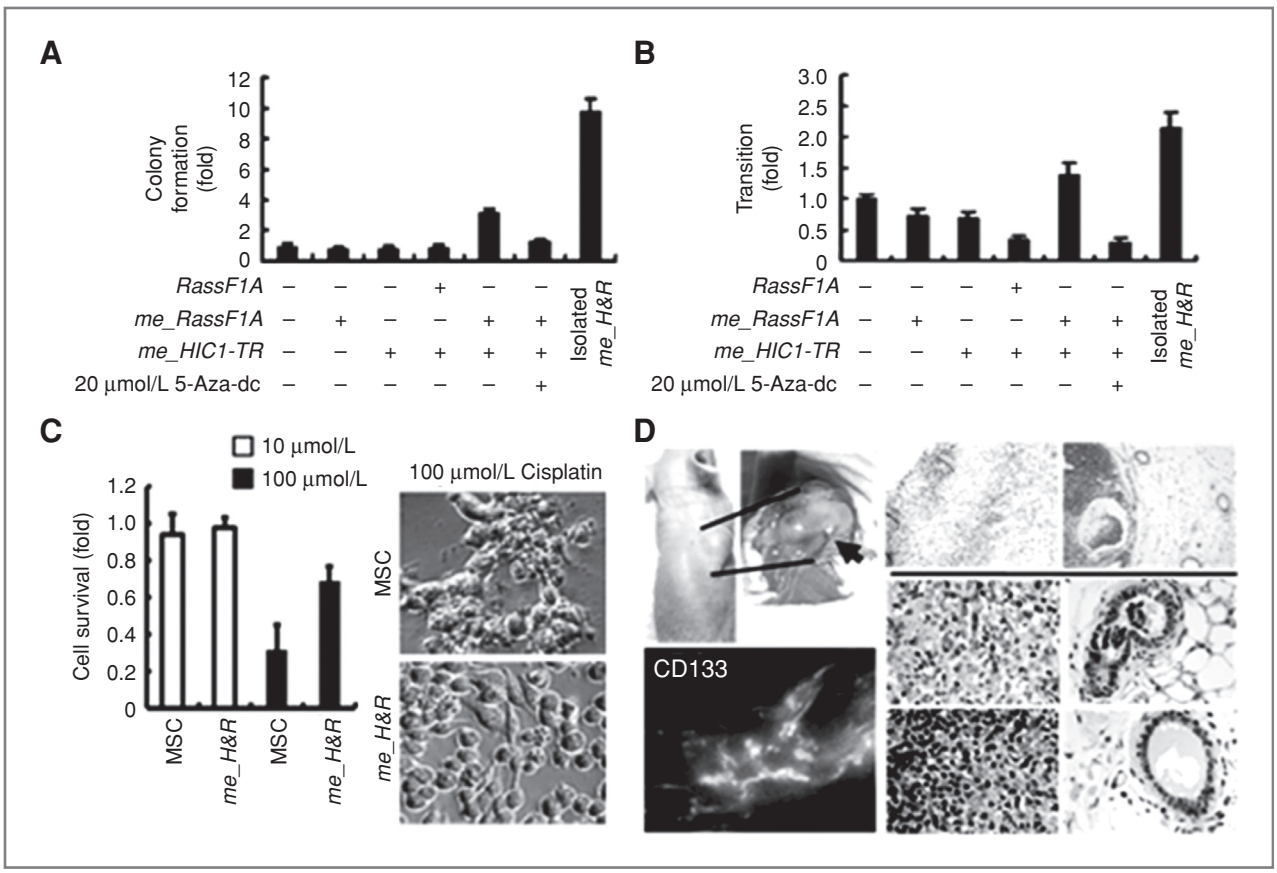

Figure 4. *In vitro* and *in vivo* tumorigenesis of *me_H&R*-transfected MSCs. A, in soft agar assays, *me_H&R*-transfected MSCs formed a greater number of colonies versus controls (5th and 7th columns), and colony formation was inhibited by 5-aza-dc treatment (6th column). B, quantification of migrated cells. *Me_H&R*-transfected MSCs migrated to the bottom of the Transwell inserts (control cells did not) and this migration was blocked by 5-aza-dc treatment. C, increased drug resistance in *me_H&R*-transfected MSCs. Cisplatin-induced cell death was measured by MTT assay. High dose cisplatin treatment (100 mmol/L) caused massive cell death in control MSCs but not in *me_H&R*-transfected MSCs (histogram). Representative images of cisplatin-induced cell death (right). D, tumor development in mice inoculated with *me_H&R*-transfected MSCs ($n = 9$; left top). H&E staining (right) and immunohistochemistry of CD133 expression (bottom left) were carried out on xenograft tumors.

Published OnlineFirst April 25, 2011; DOI:10.1158/0008-5472.CAN-10-3418

osteogenic differentiation. MSCs transfected with *me_H&R* were able to differentiate into neuron-like cells (Fig. 3D, right, indicated by NeuN staining) and osteoblasts (Fig. 3D, left bottom, alkaline phosphatase positive). These data indicate that although concurrent methylation of *HIC1* and *RassF1A* TSGs was sufficient to transform MSCs, as indicated by altered anchorage dependence and methylation patterns, the transformed MSCs retained somatic stem cell characteristics.

The proliferation and invasion capability of transformed MSCs were evaluated by using colony formation and Transwell studies. Colony formation was substantially increased (~8-fold, $n = 6$) in *me_H&R*-transfected cells versus controls (Fig. 4A and Supplementary Figs. S8A and S9A), and this was inhibited by 5-aza-dc treatment (Fig. 4A and Supplementary Fig. S8A). In Transwell studies, MSCs transfected with *me_H&R* exhibited greater migratory capability (Fig. 4B and

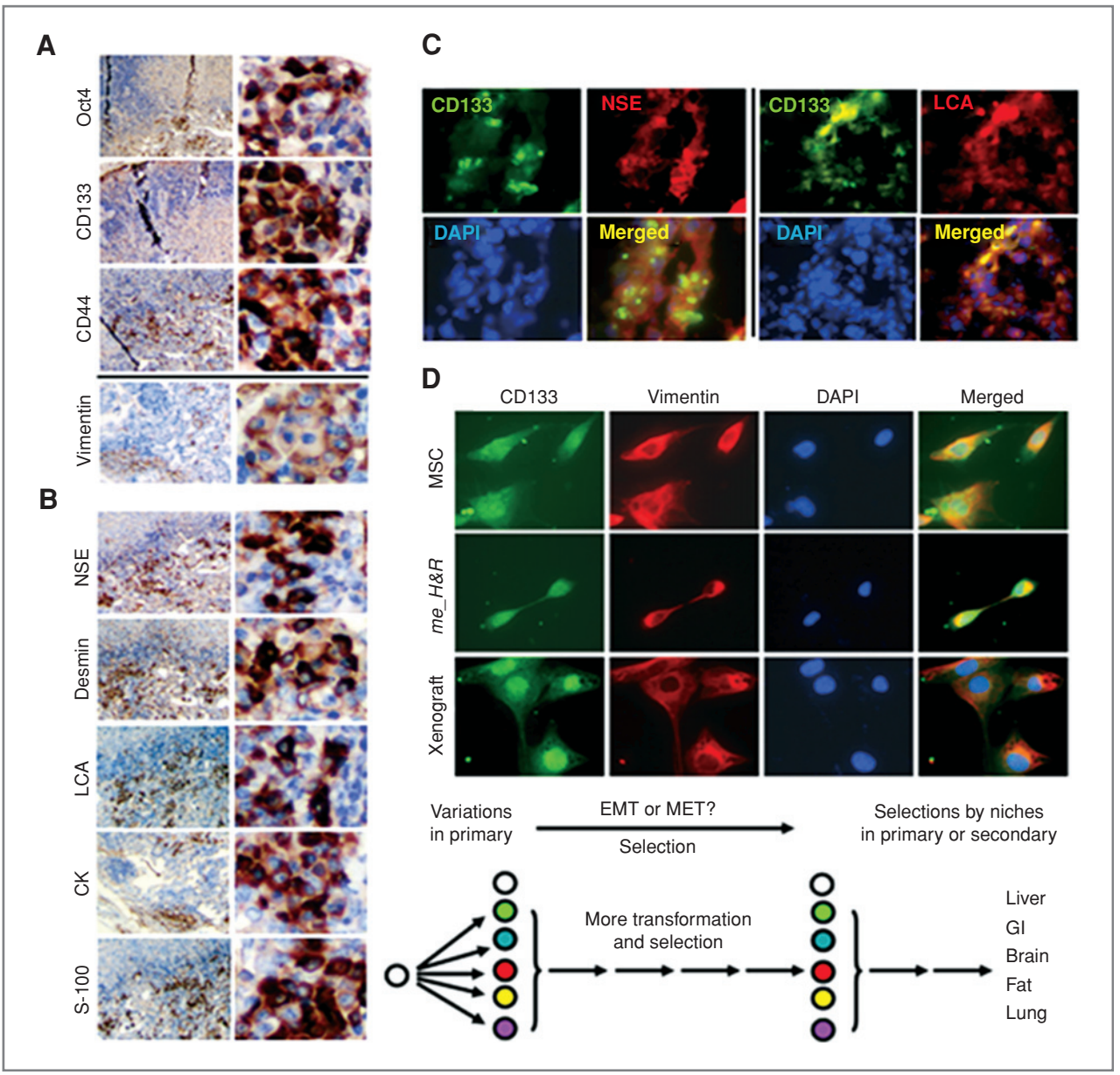

Figure 5. Immunohistochemistry of xenografts from *me_H&R*-transfected MSCs. A, stem cell marker expression in xenografts. Representative images of cells positive for CD44, CD133, or Oct4 from the serial sections of xenograft tumors. B, representative images from xenografts ($n = 36$) containing heterogeneous cell types of either epithelial or mesenchymal lineage (vimentin). C, expression of lineage-specific markers (left: NSE, right: LCA) was observed in many CD133-positive cells, or lineage-specific marker expressing cells surrounded CD133-positive cells. D, top, images of coexpression of CD133 and vimentin in a subpopulation of control MSCs (top), *me_H&R*-transfected MSCs (middle), and subcultures derived from *me_H&R*-transfected MSC xenografts (bottom). Bottom, simplified model for mechanisms by which normal somatic stem cells (primary) can gradually become tissue-specific tumor cells, via transformation and clonal selection occurring at niches in primary or secondary sites. Colored circles represent different lineages. EMT: epithelial-to-mesenchymal transition; GI, gastrointestine.

Published OnlineFirst April 25, 2011; DOI:10.1158/0008-5472.CAN-10-3418

Supplementary Figs. S8B and S9B). Taken together, these results indicated that MSCs with concurrent methylation of *HIC1* and *RassF1A* acquired a cancer phenotype.

Acquired drug resistance is a hallmark of malignancy and a characteristic of a cancer stem cell (CSC) phenotype. Cisplatin treatment induced cell death in control MSCs in a dose-dependent manner, but the drug was much less effective in *me_H&R*-transfected MSCs, even at a very high dose (100 μmol/L; Fig. 4C), further indicating that concurrent *HIC1* and *RassF1A* methylation transformed normal somatic stem cells into CSC like.

To examine the tumorigenic capacity of the *me_H&R*-transfected MSCs *in vivo*, immunodeficient nude mice were inoculated with *me_H&R*-treated MSCs. As shown in Figure 4D, 100% of these mice developed tumors ($n = 9$), whereas the mice inoculated with control MSCs remained tumor free. Immunohistochemistry revealed the presence of $CD133^+$ stem cells in the tumors (Fig. 4D, bottom left). Furthermore, the tumors were soft tissue sarcomas like (Figs. 4D, right and 5A and B), consistent with this type of malignancy in mice with heterozygous disruption of *HIC1* (17).

Expression of stem cell markers in *me_H&R* MSC-derived tumors

We examined xenografts from serial transplantations for expression of known stem cell markers by immunohistochemistry. As shown in Figure 5A, expression of CD44, CD133, and Oct4 was observed, substantiating the CSC-like phenotype. Vimentin expression was also detected, confirming the mesenchymal origin of the xenografts. Clonal expression of a panel of epithelial markers, including neuron-specific enolase (NSE), S-100, cytokeratin, desmin, and leukocyte common antigen (LCA; Fig. 5B), further showed the ability of CSCs to differentiate into heterogeneous tumors. In addition, expression of both stem cell (CD133) and mesenchymal (vimentin) markers in sparsely scattered cells of *me_H&R* tumors showed that the xenografts were derived from inoculated *me_H&R* MSCs (Fig. 5C). Although we observed slight enrichment of $CD133^+$/$vimentin^+$ cells in serial transplantation experiments (Supplementary Fig. S10A), the overall percentage remained low, in agreement with previous observations (25) that CSCs continue to form a small proportion of the overall tumor even after *in vitro* enrichment and xenograft transplantation.

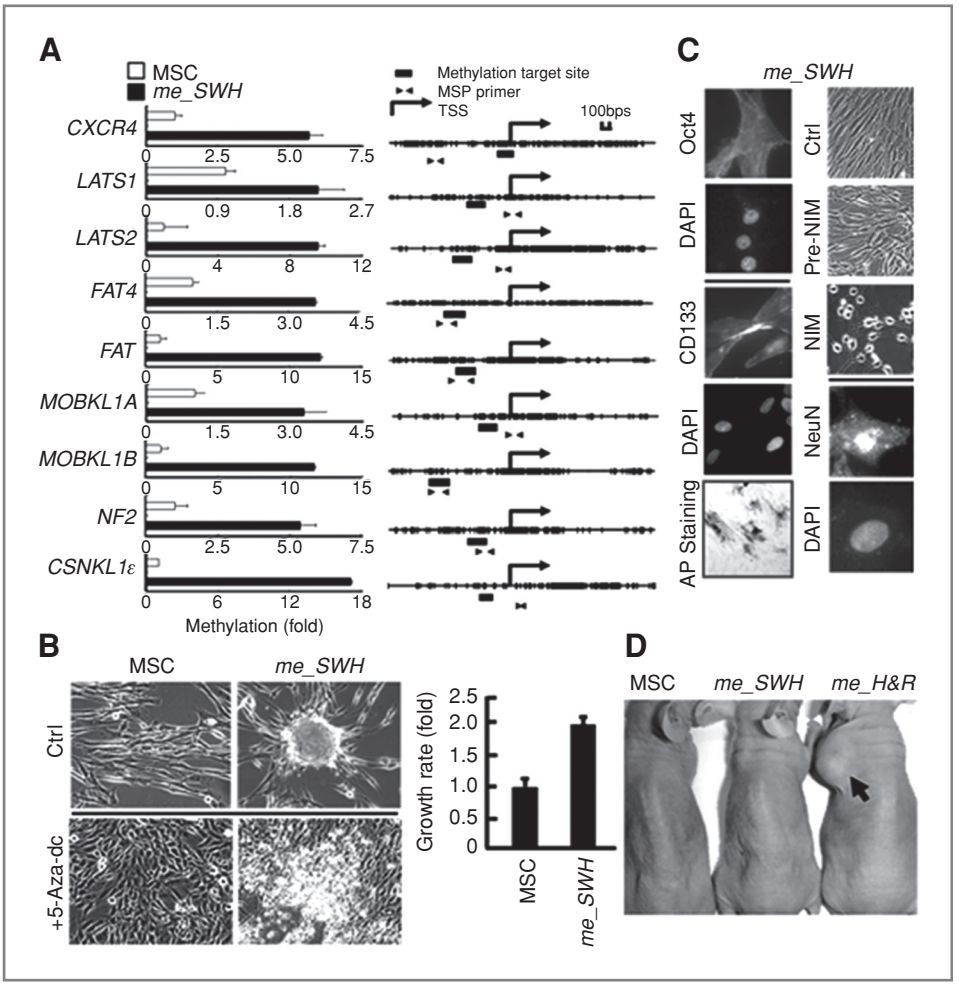

Figure 6. TDM of SWH signaling pathway is not sufficient for full MSC transformation. *In vitro* methylation of the main components within SWH pathway (*me_SWH*) was carried out and transfected cells were characterized. A, methylation of the 9 SWH pathway components was detected by qMSP. In the physical maps, short, filled boxes indicate the target sites in each promoter and the arrow heads indicate the primer sites used to detect the TDM on the left. B, images, methylation of the SWH pathway caused the MSC to lose contact inhibition (top right). Treatment with 5-aza-dc reversed the aggregate phenotype caused by TDM (bottom right). Histograms, *me_SWH*-treated MSCs exhibited higher growth rate in soft agar assay versus mock-treated cells. C, *me_SWH*-treated MSCs retained stemness properties. *Me_SWH*-treated MSCs expressed stem cell markers CD133 and Oct4 (top left) and neuronal (right) and osteogenic (bottom left) lineages could be induced. D, no tumor formation was observed after subcutaneous injection of *me_SWH*-treated MSCs in nude mice (middle; $n = 8$); in contrast, subcutaneously implanted *me_H&R*-treated MSCs formed tumors (right). TSS, transcriptional start site.

Published OnlineFirst April 25, 2011; DOI:10.1158/0008-5472.CAN-10-3418

Transformation specificity induced by concurrent methylated of *HIC1* and *RassF1A*

To establish that MSC transformation was due to concomitant methylation of *HIC1* and *RassF1A* and not accumulation of targeted genes, we simultaneously methylated 9 genes in the SWH signaling pathway by TDM in MSCs (ref. 20; Fig. 6A). Abnormal SWH signaling pathway has been associated with tumorigenesis in both mammalian cells and *Drosophila* (26, 27), and RassF1A is a SWH pathway component controlling cellular proliferation, survival, antiapoptosis, organ size, and cell contact inhibition (20, 28). Because loss of function of these 9 genes (Fig. 6A) has been reported in various cancers (20), we hypothesized that methylation of these SWH signaling pathway genes (i.e., "*me_SWH*") could cause MSC transformation. *me_SWH*-treated MSCs displayed loss of contact inhibition (Fig. 6B), increased colony formation in soft agar assays (Supplementary Fig. S9A), and were invasive in Transwell assays (Supplementary Fig. S9B). Furthermore, *me_SWH*-treated MSCs retained stemness markers and could be induced to differentiate (Fig. 6C). However, these cells were not tumorigenic in nude mice assay (Fig. 6D). Taken together, these results support a unique role for the combination of methylated *HIC1 and RassF1A* in MSC transformation. Furthermore, increasing the number of methylated loci within the SWH pathway did not result in transformation of MSC, even though *RassF1A* was included in the *me_SWH* loci.

Collectively, our data showed that concurrent methylation of *HIC1* and *RassF1A* was sufficient to transform MSCs. The observation that pluripotency was maintained suggests that the cells had acquired a CSC phenotype. Increased proliferation is often accompanied with increased genetic and/or epigenetic mutations (29), which further enhance transformation and clonal selection during mesenchymal-to-epithelial transition (MET; refs. 30–32). In more permissive environments, including nude mice, subpopulations of inoculated *me_H&R* produced NSE- and LCA-positive epithelial cells (Fig. 5C) or other cell types (Supplementary Fig. S10B). The acquired differentiation capacity, and perhaps later migratory capability, may allow these CSC-like cells to either remain in their original location or migrate to form secondary tumors (Fig. 5D, bottom scheme). Bioinformatic analysis further revealed the presence of p53 binding elements within the targets identified by DMH (Supplementary Table S3), suggesting a central role for p53 in MSC oncogenic transformation. The tumor suppressor activities of both HIC1 and RassF1A are due, in part, to p53 activation, in agreement with previous genetic findings (17). Concordant silencing of *HIC1* and *RassF1A* by DNA methylation may impair p53-mediated apoptosis and contribute to the tumorigenic ability of MSCs.

Discussion

Here, we elucidated the role of DNA methylation in the transformation of somatic stem cells into CSC-like cells. Bone marrow–derived MSCs are known to play important roles in cancer progression and metastasis (33–35). By providing a microenvironment that enhances primary tumor growth, invasiveness, and metastasis, MSCs have the capacity to mobilize to other organs, providing a niche suitable for the disseminated cancer cells to metastasize to distant tissues (33). Our data show that in addition to these 2 supporting roles, MSCs may play a previously unidentified role in tumorigenesis, as abnormal DNA hypermethylation of *HIC1* and *RassF1A*, 2 TSGs involved in functionally diverse, interacting networks, transformed MSCs from normal somatic stem cells to cancer-like stem cells.

Concordant methylation of *HIC1* and *RassF1A* has been identified in advanced ovarian cancer (36), and *HIC1* shows increased concurrent hypermethylation with other genes in advanced myelodysplasia syndrome (37), suggesting that disturbance of *HIC1*-associated networks may be essential for tumor initiation. Unlike *RassF1A*, which can be inactivated by either genetic or epigenetic mechanisms, repression of *HIC1* is mainly caused by DNA methylation (16). Thus, DNA hypermethylation of *HIC1* could predispose cells to cancer development (Fig. 2A). A second epigenetic hit, such as *RassF1A* methylation, may then permit more efficient cancer development. However, it is also possible that hypermethylation of *RassF1A* results in further epigenomic disturbances, rendering a cell more susceptible to cancer-causing insult(s). Our data further show that DNA methylation is a cause rather than a consequence of malignancy, and p53 may be at the center of this oncogenic transformation. p53-dependent apoptosis plays an integral part in tumor growth, progression, and drug resistance development (38), and the tumor suppressor ability of both HIC1 and RassF1A is due to p53 activation. Thus, concordant silencing of *HIC1* and *RassF1A* by DNA methylation may synergistically disrupt the p53-mediated apoptotic pathway and contribute to the observed tumorigenic ability of MSCs.

The origin of CSCs or cancer-initiating cells has been widely debated. These cells may arise either from deregulated somatic stem cells or from dedifferentiated mature cells (4, 7, 8, 39–42). It has been reported that several hypermethylated genes, including *HIC1* and *RassF1A*, in adult cancer are unmethylated in embryonic stem cells and only partially methylated in embryonic carcinomas (43). In this study, we show that forced epigenetic silencing of *HIC1* and *RassF1A* is sufficient to confer normal somatic stem cells with malignant properties, including loss of contact inhibition, increased colony formation, migration capability, drug resistance, and tumor formation in inoculated mice. Moreover, the cells retained sensitivity to neuron- and osteocyte-induction and displayed both lineage-specific markers and stem cell markers in xenografts. Thus, we reason that methylation of both *HIC1* and *RassF1A* triggers the transformation of normal somatic stem cells to CSC-like cells. As proposed in Figure 5D, this transition may promote additional transforming events and further cellular selection. We further propose that under the influence of different environmental niches, these transformed stem cells could give rise to tissue-specific cancers.

Disclosure of Potential Conflicts of Interest

No potential conflicts of interest were disclosed.

Published OnlineFirst April 25, 2011; DOI:10.1158/0008-5472.CAN-10-3418

Grant Support

Y.-W. Leu (NRPGM, NSC-98-3112-B-194-001 and NSC-97-2320-B-194-003-MY3), S.-H. Hsiao (NSC-96-2320-B-194-004), and S.-J. Tsai and Y.-W. Leu (NSC-97-2627-B-006-003) are supported by the National Science Council, Taiwan. K.P. Nephew and T.H.-M. Huang are supported in part by NIH grants CA085289 and CA113001.

The costs of publication of this article were defrayed in part by the payment of page charges. This article must therefore be hereby marked *advertisement* in accordance with 18 U.S.C. Section 1734 solely to indicate this fact.

Received September 17, 2010; revised March 27, 2011; accepted April 18, 2011; published OnlineFirst April 25, 2011.

References

1. Baylin S. DNA methylation and epigenetic mechanisms of carcinogenesis. Dev Biol 2001;106:85–7.
2. Esteller M. Epigenetics in cancer. N Engl J Med 2008;358:1148–59.
3. Feinberg AP, Tycko B. The history of cancer epigenetics. Nat Rev Cancer 2004;4:143–53.
4. Balch C, Nephew KP, Huang TH, Bapat SA. Epigenetic "bivalently marked" process of cancer stem cell-driven tumorigenesis. Bioessays 2007;29:842–5.
5. Baylin SB, Ohm JE. Epigenetic gene silencing in cancer–a mechanism for early oncogenic pathway addiction?Nat Rev Cancer 2006;6:107–16.
6. Bird A. DNA methylation patterns and epigenetic memory. Genes Dev 2002;16:6–21.
7. Feinberg AP. Phenotypic plasticity and the epigenetics of human disease. Nature 2007;447:433–40.
8. Jones PA, Baylin SB. The epigenomics of cancer. Cell 2007;128:683–92.
9. Eden A, Gaudet F, Waghmare A, Jaenisch R. Chromosomal instability and tumors promoted by DNA hypomethylation. Science 2003;300:455.
10. Gaudet F, Hodgson JG, Eden A, Jackson-Grusby L, Dausman J, Gray JW, et al. Induction of tumors in mice by genomic hypomethylation. Science 2003;300:489–92.
11. Hsiao SH, Lee KD, Hsu CC, Tseng MJ, Jin VX, Sun WS, et al. DNA methylation of the Trip10 promoter accelerates mesenchymal stem cell lineage determination. Biochem Biophys Res Commun 2010;400:305–312.
12. Hsu CC, Li HP, Hung YH, Leu YW, Wu WH, Wang FS, et al. Targeted methylation of CMV and E1A viral promoters. Biochem Biophys Res Commun 2010;402:228–234.
13. Rosland GV, Svendsen A, Torsvik A, Sobala E, McCormack E, Immervoll H, et al. Long-term cultures of bone marrow-derived human mesenchymal stem cells frequently undergo spontaneous malignant transformation. Cancer Res 2009;69:5331–9.
14. Torsvik A, Rosland GV, Svendsen A, Molven A, Immervoll H, McCormack E, et al. Spontaneous malignant transformation of human mesenchymal stem cells reflects cross-contamination: putting the research field on track–letter. Cancer Res 2010;70:6393–6.
15. Rubio R, Garcia-Castro J, Gutierrez-Aranda I, Paramio J, Santos M, Catalina P, et al. Deficiency in p53 but not retinoblastoma induces the transformation of mesenchymal stem cells *in vitro* and initiates leiomyosarcoma *in vivo*. Cancer Res 2010;70:4185–94.
16. Chen W, Cooper TK, Zahnow CA, Overholtzer M, Zhao Z, Ladanyi M, et al. Epigenetic and genetic loss of Hic1 function accentuates the role of p53 in tumorigenesis. Cancer Cell 2004;6:387–98.
17. Chen WY, Zeng X, Carter MG, Morrell CN, Chiu Yen RW, Esteller M, et al. Heterozygous disruption of Hic1 predisposes mice to a gender-dependent spectrum of malignant tumors. Nat Genet 2003;33:197–202.
18. Leu YW, Rahmatpanah F, Shi H, Wei SH, Liu JC, Yan PS, et al. Double RNA interference of DNMT3b and DNMT1 enhances DNA demethylation and gene reactivation. Cancer Res 2003;63:6110–5.
19. Fleuriel C, Touka M, Boulay G, Guerardel C, Rood BR, Leprince D. HIC1 (hypermethylated in cancer 1) epigenetic silencing in tumors. Int J Biochem Cell Biol 2009;41:26–33.
20. Harvey K, Tapon N. The Salvador-Warts-Hippo pathway–an emerging tumour-suppressor network. Nat Rev Cancer 2007;7:182–91.
21. Lee KD, Kuo TK, Whang-Peng J, Chung YF, Lin CT, Chou SH, et al. *In vitro* hepatic differentiation of human mesenchymal stem cells. Hepatology 2004;40:1275–84.
22. Yan PS, Venkataramu C, Ibrahim A, Liu JC, Shen RZ, Diaz NM, et al. Mapping geographic zones of cancer risk with epigenetic biomarkers in normal breast tissue. Clin Cancer Res 2006;12:6626–36.
23. Yan PS, Wei SH, Huang TH. Differential methylation hybridization using CpG island arrays. Methods Mol Biol 2002;200:87–100.
24. Palakurthy RK, Wajapeyee N, Santra MK, Gazin C, Lin L, Gobeil S, et al. Epigenetic silencing of the RASSF1A tumor suppressor gene through HOXB3-mediated induction of DNMT3B expression. Mol Cell 2009;36:219–30.
25. Zhang S, Balch C, Chan MW, Lai HC, Matei D, Schilder JM, et al. Identification and characterization of ovarian cancer-initiating cells from primary human tumors. Cancer Res 2008;68:4311–20.
26. Bennett FC, Harvey KF. Fat cadherin modulates organ size in Drosophila via the Salvador/Warts/Hippo signaling pathway. Curr Biol 2006;16:2101–10.
27. Meignin C, Alvarez-Garcia I, Davis I, Palacios IM. The salvador-warts-hippo pathway is required for epithelial proliferation and axis specification in Drosophila. Curr Biol 2007;17:1871–8.
28. Polesello C, Tapon N. Salvador-warts-hippo signaling promotes Drosophila posterior follicle cell maturation downstream of notch. Curr Biol 2007;17:1864–70.
29. Hsiao SH, Huang TH, Leu YW. Excavating relics of DNA methylation changes during the development of neoplasia. Semin Cancer Biol 2009;19:198–208.
30. Tsuji T, Ibaragi S, Hu GF. Epithelial-mesenchymal transition and cell cooperativity in metastasis. Cancer Res 2009;69:7135–9.
31. Huber MA, Kraut N, Beug H. Molecular requirements for epithelial-mesenchymal transition during tumor progression. Curr Opin Cell Biol 2005;17:548–58.
32. Yang J, Weinberg RA. Epithelial-mesenchymal transition: at the crossroads of development and tumor metastasis. Dev Cell 2008;14:818–29.
33. Hu M, Polyak K. Microenvironmental regulation of cancer development. Curr Opin Genet Dev 2008;18:27–34.
34. Karnoub AE, Dash AB, Vo AP, Sullivan A, Brooks MW, Bell GW, et al. Mesenchymal stem cells within tumour stroma promote breast cancer metastasis. Nature 2007;449:557–63.
35. Serakinci N, Guldberg P, Burns JS, Abdallah B, Schrodder H, Jensen T, et al. Adult human mesenchymal stem cell as a target for neoplastic transformation. Oncogene 2004;23:5095–8.
36. Teodoridis JM, Hall J, Marsh S, Kannall HD, Smyth C, Curto J, et al. CpG island methylation of DNA damage response genes in advanced ovarian cancer. Cancer Res 2005;65:8961–7.
37. Aggerholm A, Holm MS, Guldberg P, Olesen LH, Hokland P. Promoter hypermethylation of p15INK4B, HIC1, CDH1, and ER is frequent in myelodysplastic syndrome and predicts poor prognosis in early-stage patients. Eur J Haematol 2006;76:23–32.
38. Kerr JF, Winterford CM, Harmon BV. Apoptosis. Its significance in cancer and cancer therapy. Cancer 1994;73:2013–26.
39. Bjerkvig R, Tysnes BB, Aboody KS, Najbauer J, Terzis AJ. Opinion: the origin of the cancer stem cell: current controversies and new insights. Nat Rev Cancer 2005;5:899–904.
40. Gupta PB, Chaffer CL, Weinberg RA. Cancer stem cells: mirage or reality? Nat Med 2009;15:1010–2.
41. Pardal R, Clarke MF, Morrison SJ. Applying the principles of stem-cell biology to cancer. Nat Rev Cancer 2003;3:895–902.
42. Wicha MS, Liu S, Dontu G. Cancer stem cells: an old idea–a paradigm shift. Cancer Res 2006;66:1883–90.
43. Ohm JE, McGarvey KM, Yu X, Cheng L, Schuebel KE, Cope L, et al. A stem cell-like chromatin pattern may predispose tumor suppressor genes to DNA hypermethylation and heritable silencing. Nat Genet 2007;39:237–42.
44. van Iersel MP, Kelder T, Pico AR, Hanspers K, Coort S, Conklin BR, et al. Presenting and exploring biological pathways with PathVisio. BMC Bioinformatics 2008;9:399.